Optics Letters

Real-time, label-free, and fast monitoring of cell viability by an optical fiber-based microcantilever biosensor

Famei Wang,[1] Jiabin Huang,[2] Jie Zhou,[3] Hanlin Xu,[1] Xiaoyang Guo,[1] Zhe Zhang,[1] Jun Yu,[1] Qingdian Lin,[1] Cangtao Zhou,[1] Chao Liu,[4] Paul K. Chu,[5] and Changrui Liao[2,*]

[1]Shenzhen Key Laboratory of Ultra-Intense Laser and Advanced Material Technology, Center for Intense Laser Application Technology, College of Engineering Physics, Shenzhen Technology University, Shenzhen 518118, China
[2]Shenzhen Key Laboratory of Ultrafast Laser Micro/Nano Manufacturing, Key Laboratory of Optoelectronic Devices and Systems of the Ministry of Education/Guangdong Province, College of Physics and Optoelectronic Engineering, Shenzhen University, Shenzhen 518060, China
[3]College of Laboratory Medicine, Hubei University of Chinese Medicine, Wuhan, China
[4]School of Electronics Science, Northeast Petroleum University, Daqing 163318, China
[5]Department of Physics, Department of Materials Science and Engineering, and Department of Biomedical Engineering, City University of Hong Kong Hong Kong SAR, Tat Chee Avenue, Kowloon, Hong Kong, China
*cliao@szu.edu.cn

Received 15 May 2025; revised 10 July 2025; accepted 13 July 2025; posted 14 July 2025; published 7 August 2025

To overcome the difficulty of effective, real-time, and rapid detection of cell activities in biological experiments, an optical fiber-based microcantilever biosensor is designed and prepared using microelectromechanical system (MEMS) technology. The cantilever beam is integrated with a single-mode fiber to form a Fabry–Perot interferometer (FPI). After the cells attach to the cantilever, changes in the resonance wavelengths of the interference spectra are monitored to detect the cantilever fluctuations caused by cell movements. We report for the first time, to the best of our knowledge, the use of optical fiber interference demodulation detection to assess cell viability continuously and directly in the cell culture medium. The device delivers excellent performance in detecting the effects of doxorubicin on the activity of HeLa cells. The high detection sensitivity stems from the cantilever with a spring constant of 0.12 N/m. It takes about 2 hours to assess the reactions between cancer cells and anticancer drugs. This breakthrough technology establishes a new paradigm for high-throughput drug screening, dynamic resistance evaluation, and mechanobiological studies, with significant potential in clinical diagnostics and personalized therapeutics development.

https://doi.org/10.1364/OL.567440

Cell viability measurement is needed to determine the survival state and activity of cells [1–3], cell growth [4,5], proliferation [6], and metabolism [7,8]. Besides biomedical fields, the determination of cell activity is important in tissue engineering [9], treatment of living cells [10], and research [11]. Cell-based assays are usually used to screen compounds to determine their possible effects on cell proliferation or cytotoxicity [12]. For example, in cancer research, the response of tumors to treatment can be evaluated by detecting the activity of tumor cells [13–15]. To evaluate the safety of new drugs, a variety of *in vitro* cell-based detection methods are used. However, current *in vitro* cell-based detection methods are time-consuming and costly and require skilled personnel [16].

Microcantilever sensors enable label-free, real-time detection of biomolecules (proteins, nucleic acids, etc.) through surface stress-induced bending in static mode [17–19]. Compared to traditional methods like atomic force microscopy, our optical fiber-based integrated microcantilever biosensor, fabricated by scalable MEMS technology, cuts costs and is highly compact. The core sensing part is only a few square millimeters, and the whole setup is over ten times smaller than commercial AFMs, rendering it highly practical in many applications [20–22]. This synergy enhances cell activity and drug resistance detection capabilities through improved integration and signal stability.

In this study, an optical fiber end-face microcantilever cell sensor is designed and demonstrated for *in vitro* monitoring of cell viability. The key innovation lies in the monolithic integration of a MEMS-fabricated low-spring-constant microcantilever (0.12 N/m) directly into a single-mode optical fiber to form a highly compact Fabry–Perot interferometer (FPI). This unique design eliminates complex free-space optics and enables direct cell monitoring in culture medium *via* optical interference demodulation of cantilever deflections induced by cellular activity (Fig. 1(a)). This technique, which achieves high-sensitivity detection of cell viability dynamics within just 2 h, as demonstrated by the doxorubicin effects on HeLa cells, not only overcomes the limitations of existing cell activity detection methods but also opens up new avenues for high-throughput drug screening, dynamic drug resistance evaluation, mechanobiolog-

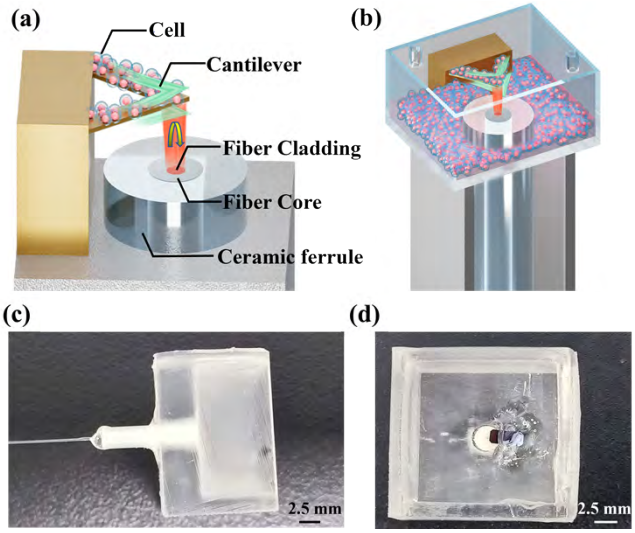

Fig. 1. (a) Working principle of detecting microcantilever motions by an optical interferometer. (b) Schematic diagram of the cell activity sensor. (c), (d) Side view and top view of the sensor.

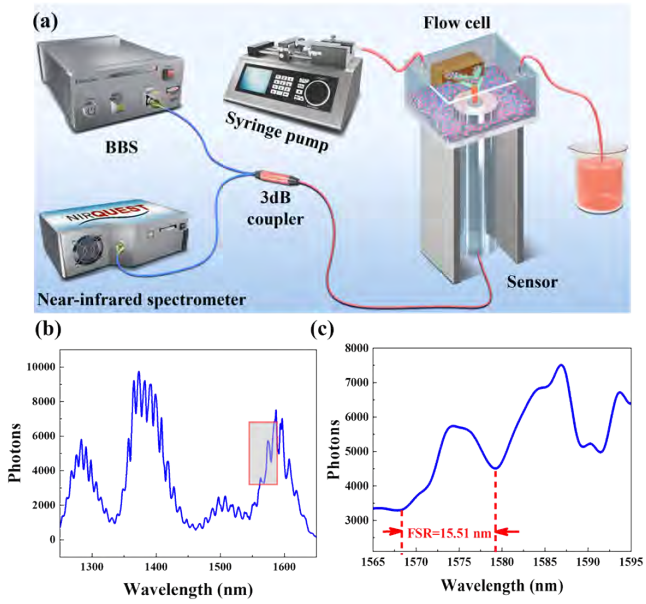

Fig. 2. (a) Schematic representation of the optical fiber-based microcantilever biosensor system. Reflection spectra of cell viability sensor (b) 1250–1650 nm and (c) 1565–1590 nm.

ical research, clinical diagnostics, and personalized medicine development.

As shown in Fig. 1(a), the F-P sensor comprises a single-mode fiber (SMF) and microcantilever assembled on the fiber end face, forming an FPI between the fiber end face and the cantilever lower surface, where the cavity length critically impacts performance. To improve the sensitivity of the sensor while obtaining high contrast interference spectra, Eq. (1) is used [21]:

$$FSR = |\lambda_{m+1} - \lambda_m| = \frac{\lambda_{m+1}\lambda_m}{2nL}, \tag{1}$$

where λ_{m+1} and λ_m are the adjacent resonant wavelength, L is the cavity length of the F-P cavity, and n is the refractive index of the cavity medium of the F-P cavity.

When the probe is subjected to a force, the microcantilever beam bends, altering the optical path difference of the F-P cavity and shifting the interference fringes. The deflection of the microcantilever can be determined by detecting the resonant wavelength of the peak or valley in the interference spectrum. The corresponding relationship between the wavelength change ($\Delta\lambda$) and cavity length of the F-P cavity change (ΔL) can be simplified as follows [22]:

$$\frac{\Delta\lambda}{\lambda} = \frac{\Delta L}{L}. \tag{2}$$

The change in the cavity length can be inferred by monitoring the drift of the interference spectrum, and then the external force exerted on the probe can be measured. The biosensor immobilizes cells *via* cantilever surface chemical modification. The cell movement produces cantilever bending (deflection) as point loads to enable cell activity monitoring by monitoring the time-dependent deflection changes.

A Bruker NP-O10 triangular cantilever (k = 0.12 N/m) was functionalized through sequential chemical treatments to enable cell immobilization. Initial piranha solution etching (3:1 H_2SO_4:H_2O_2, 15 min) was followed by APTES silanization (5%, 15 min) to establish amine-rich surfaces. Cell adhesion was achieved through carboxyl-amine covalent conjugation between membrane proteins and functionalized surfaces. As shown in Fig. 1(b), the bottom surface of the flow cell supported the microcantilever beam, with a ceramic ferrule fixed in its channel using UV adhesive. A single-mode fiber (SMF) with a flat end, unpeeled for protection, was inserted into a 250-μm ceramic core, and its tip was aligned with the SMF core (offset ≤10 μm) under a microscope to form an FPI. The FPI cavity length, critical for performance, was maintained at 50–100 μm to ensure interference contrast ≥6 dB and FSR of 12–25 nm at 1,550 nm, determined by Eq. (1). Figure 2(a) shows the experimental setup of the optical fiber-based microcantilever biosensor. The incident light emitted from a broadband light source (BBS) passed through a 3-dB coupler to reach the sensor. The reflected light from the sensor then passed through the same 3 dB coupler before entering the near-infrared spectrometer. Reflection spectra between 1,250 nm and 1,650 nm were acquired, as shown in Fig. 2(b). The FSR of the sensor at 1,575 nm was 15.51 nm and met the requirements, as shown in Fig. 2(c). The spectrometer recorded the reflection spectra at a frequency of 50 Hz, and the spectral data were input into Matlab for interpolation and smoothing.

Figures 3(a)–3(c) depict the microscopic images of the cells attached to the cantilever for concentrations of 1×10^7, 5×10^7, and 1×10^8 cells/mL. When the cell concentration is 1×10^7 cells/mL, there are only a few cells on the microcantilever beam. When the concentration is increased to 5×10^7 cells/mL, the number of cells on the beam increases significantly, nearly covering its entire surface. However, at a concentration of 1×10^8 cells/mL, almost no cells remain on the microcantilever. This phenomenon occurs because the flow cell has a limited volume of 1 mL, which can only accommodate a small amount of cell culture medium. At high cell concentrations, prolonged incubation at 37 °C causes the medium to evaporate, resulting in cell death.

The deflection of the cantilever beam at different concentrations is shown in Fig. 4(a). The deflection variation in blank cell

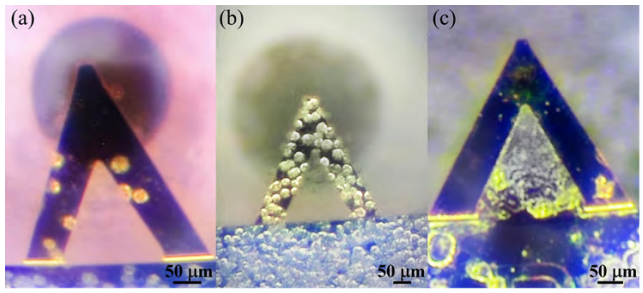

Fig. 3. Number of cells on the cantilever for different concentrations: (a) 1×10^7 cells/mL, (b) 5×10^7 cells/mL, and (c) 1×10^8 cells/mL, together with the microscopic images of the cantilever beam.

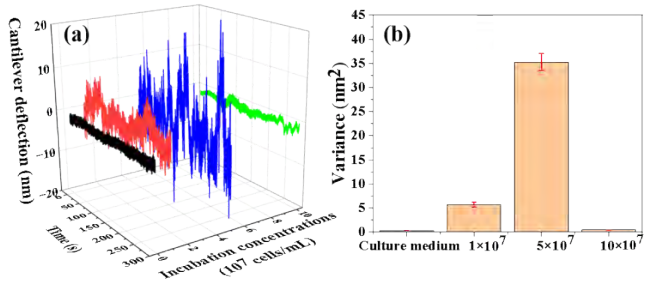

Fig. 4. Deflections of the cantilever for different incubation concentrations of HeLa cells: (a)–(d) Deflection curves of the cantilever beam: (a) 0 cells/mL (black curve), 1×10^7 cells/mL (red curve), 5×10^7 cells/mL (blue curve), and 10×10^7 cells/mL (green curve). (b) Variance of cantilever deflections.

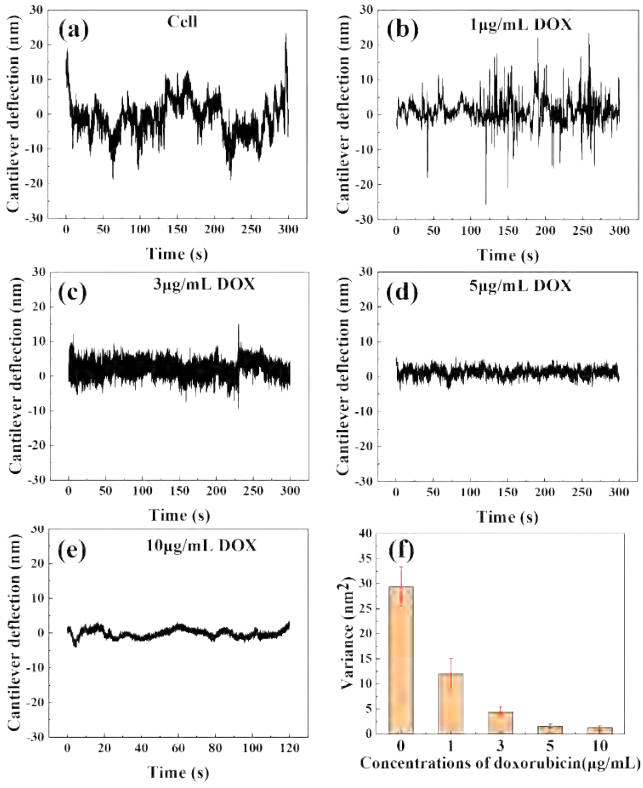

Fig. 5. Response of HeLa cells to adriamycin. HeLa cells are cultured in (a) cell culture medium, (b) 1 μg/mL, (c) 3 μg/mL, (d) 5 μg/mL, and (e) 10 μg/mL doxorubicin. (e) Variance of the deflections of the cantilever and standard deviation of three measurements under the above conditions.

culture medium is small, with a variance of only 0.27 nm^2, as shown in Fig. 4(a). At 1×10^7 cells/mL, the cantilever fluctuation increases slightly, with a deflection variance of 5.72 nm^2. At 5×10^7 cells/mL, the fluctuation becomes more pronounced, with the variance reaching 35.23 nm^2. At 10×10^7 cells/mL, the fluctuation returns to a level similar to the blank medium, with a variance of 0.42 nm^2. These results are consistent with microscopic observations, confirming the relationship between cell concentration and cantilever behavior.

Based on these findings, a cell concentration of 5×10^7 cells/mL was selected for subsequent experiments. To evaluate HeLa cells' response to doxorubicin, a 5×10^7 cells/mL suspension is injected into a flow cell and incubated. After injecting cell culture medium with a determined doxorubicin concentration into the flow cell and standing for 1 h, the sensor treated with doxorubicin is marked as 1 μg/mL, 3 μg/mL, 5 μg/mL, and 10 μg/mL.

Figure 5 shows the dose-dependent suppression of the HeLa cell activity by doxorubicin (DOX) measured by the same biosensor. Cell attachment leads to significant cantilever fluctuations (deflection variance: 29.46 nm^2). As shown in Figs. 5(b)–5(e), DOX treatment causes a concentration-dependent decrease in these fluctuations. The deflection variance drops to 12.1 nm^2 (58.9% reduction) at 1 μg/mL, 4.46 nm^2 (84.9% reduction) at 3 μg/mL, 1.53 nm^2 (94.8% reduction) at 5 μg/mL, and 1.27 nm^2 (95.7% reduction) at 10 μg/mL. Near-abolished fluctuations at ≥5 μg/mL indicate cell death. The average deflection variance and standard deviation from three independent measurements (Fig. 5(f)) confirm that the HeLa cell activity diminishes progressively with increasing DOX concentration. Rigorous sensor regeneration between concentration tests (validated by consistent baseline variance recovery) ensures reliable concentration-dependent data, confirming the effectiveness in anticancer drug screening.

To further validate the sensor viability, Fig. 6 presents deflection curves and variance over time following treatment with 10 μg/mL doxorubicin, monitored at 30-minute intervals between 1 and 2.5 h post-addition (5-minute tests per interval). One hour after treatment, deflection variance drops to 9.11 nm^2 (69.1% reduction from control) and further to 4.43 nm^2 (85% reduction) after 1.5 h. After 2 and 2.5 h, fluctuations nearly cease, with variances of 1.02 nm^2 (96.5% reduction) and 1.81 nm^2 (93.9% reduction), respectively. The time-dependent variance decrease mirrors amphotericin B addition, confirming reduced HeLa cell activity and eventual death. These results highlight the sensor's capability for real-time monitoring and quantitative assessment of anticancer drug effects within 2 h.

To demonstrate the clinical viability, a real-time, label-free optical fiber microcantilever biosensor is constructed for rapid detection of cell viability. The sensor quantifies cellular activities by monitoring resonance wavelength shifts from cantilever deflections. It requires neither labeling nor complex instrumentation. Practicality is validated by dynamically profiling HeLa cell responses to doxorubicin. Quantitative drug-efficacy data within 2 h offers a speed advantage over traditional endpoint assays (e.g., MTT/XTT/CCK-8), which typically require 24–72 h [23–26]. The compact design, low cost, high sen-

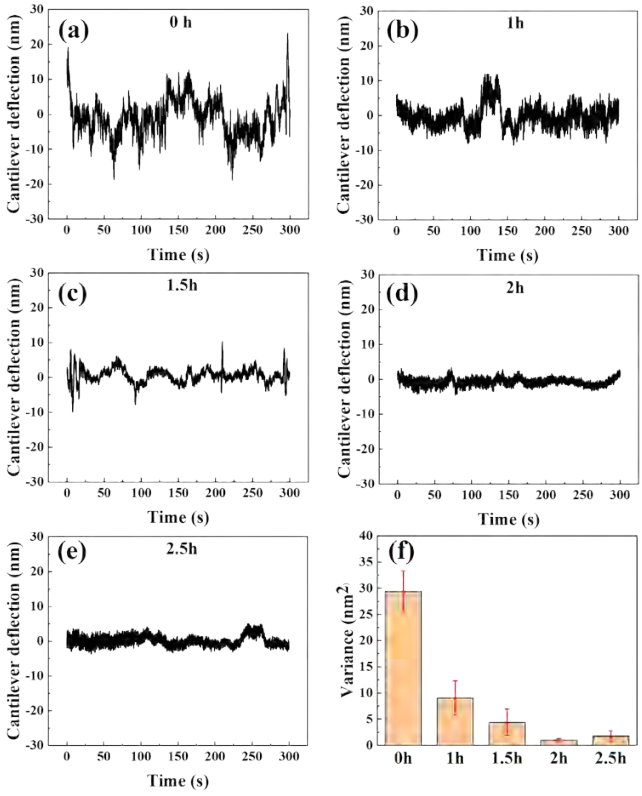

Fig. 6. Effects of doxorubicin time on the activity of HeLa cells: (a) Deflection changes with time without adriamycin. Deflection changes after adding 10 μg/mL adriamycin for (b) 1 h, (c) 1.5 h, (d) 2 h, and (e) 2.5 h. (e) Variance and standard deviation of three measurements in the above time periods.

sitivity (0.12 N/m cantilever), and rapid response outperform conventional *in vitro* methods in efficiency and integration. Future work will enhance biocompatibility via long-term studies, enable multiplexed cantilever arrays detection, miniaturize the platform for organ-on-chip integration, and detect mechanophenotypic responses to diverse stimuli (e.g., pathogens, toxins). These advancements will solidify the sensor's potential as a transformative tool for clinical diagnostics, personalized therapeutic development, high-throughput drug screening, dynamic drug resistance evaluation, and fundamental mechanobiological studies. All in all, this technique has large potential in clinical diagnostics, personalized therapeutics, and high-throughput drug screening.

Funding. National Natural Science Foundation of China (62305223); Basic and Applied Basic Research Foundation of Guangdong Province (2022A1515110971); China Postdoctoral Science Foundation (2022M722173); Shenzhen Science and Technology Program (ZDSYS20220606100405013); Natural Science Foundation of Heilongjiang Province (JQ2023F001); City University of Hong Kong Donations (9220061, DON-RMG 9229021).

Disclosures. The authors declare no conflicts of interest.

Data availability. Data underlying the results presented in this paper are not publicly available at this time but may be obtained from the authors upon reasonable request.

REFERENCES

1. J. N. Rosenberg and N. C. Cady, Curr. Opin. Biotechnol. **71**, 123 (2021).
2. M. J. Stoddart, Methods Mol. Biol. **740**, 1 (2011).
3. R. A. Potyrailo, J. Dieringer, V. Cotero, *et al.*, Bioelectrochem. **125**, 97 (2019).
4. I. Malanchi, A. Santamaria-Martinez, E. Susanto, *et al.*, Nature **481**, 85 (2012).
5. F. L. Crane, P. Navas, H. Low, *et al.*, J. Gerontol.: Series A Biol. Sci. Med. Sci. **68**, 368 (2013).
6. B. Trappmann, J. E. Gautrot, J. T. Connelly, *et al.*, Nat. Mater. **11**, 642 (2012).
7. F. Ishikawa, K. Ushida, K. Mori, *et al.*, Cell Death Dis. **6**, e1619 (2015).
8. B. Zhao, L. Li, L. Wang, *et al.*, Genes Dev. **26**, 54 (2012).
9. J. C. Park, Y. S. Hwang, and H. Suh, Yonsei Med. J. **41**, 836 (2000).
10. A. V. B. Pintor, L. D. Queiroz, R. Barcelos, *et al.*, Int. Endod. J. **53**, 1348 (2020).
11. J. Wang, Y. Wei, S. Zhao, *et al.*, PLoS One **12**, e0176120 (2017).
12. R. Parboosing, G. Mzobe, L. Chonco, *et al.*, Med. Chem. **13**, 13 (2017).
13. N. L. Perillo, M. E. Marcus, and L. G. Baum, J. Mol. Med. **76**, 402 (1998).
14. M. Vinken and B. J. Blaauboer, Toxicol. In Vitro **39**, 104 (2017).
15. S. Guette-Marquet, V. Saunier, L. Pilloux, *et al.*, Bioelectrochem. **156**, 108625 (2024).
16. D. Korentzelos, A. M. Clark, and A. Wells, Int. J. Mol. Sci. **21**, 7304 (2020).
17. A. C. Kohler, L. Venturelli, G. Longo, *et al.*, Cell Surf. **5**, 100021 (2019).
18. R. Kobayashi, K. Kamitani, M. Sawamura, *et al.*, IEEE Sens. J.. **23**, 12495 (2023).
19. Y. Liu, L. Schweizer, W. Wang, *et al.*, Sens. Actuators B Chem.. **178**, 621 (2013).
20. S. Q. Wu, X. L. Llu, X. R. Zhou, *et al.*, Biosens. Bioelectron. **77**, 164 (2016).
21. F. M. Wang, M. Q. Zou, C. R. Liao, *et al.*, APL Photonics **8**, 096108 (2023).
22. M. Q. Zou, C. R. Liao, S. Liu, *et al.*, Light Sci. Appl. **10**, 171 (2021).
23. M. Szostakowska, A. Trębińska-Stryjewska, E. A. Grzybowska, *et al.*, Breast Cancer Res. Treat. **173**, 489 (2019).
24. A. Trebinska-Stryjewska, O. Swiech, L. J. Opuchlik, *et al.*, ACS Omega **5**, 7979 (2020).
25. K. Lappalainen, I. Jääskeläinen, K. Syrjänen, *et al.*, Pharm. Res. **11**, 1127 (1994).
26. L. W. Deng, L. Li, H. Yang, *et al.*, J. Nanosci. Nanotechnol. **14**, 2947 (2014).